

XuanCuong NGUYEN ^{1,2}, Yoshio ARAI¹, Wakako ARAKI ³

Effect of friction on the buckling behavior of shallow spherical shells contacting with rigid walls

Received 24 August 2023, Revised 16 January 2024, Accepted 8 February 2024, Published online 25 March 2024

Keywords: buckling map, buckling mode, friction, nonlinear buckling, shallow spherical shells

This paper investigates the effect of friction on the buckling behavior of a thin, shallow, elastic spherical shell under uniform external pressure based on an axisymmetric model of the finite element method. The study examines a combination of different geometric parameters with three different types of boundary conditions: clamped, hinged, and frictional ends with a wide range of friction coefficients. Friction has a significant influence on the buckling response of the spherical shell for all geometric parameters. In general, the critical pressure decreases as the friction coefficient or geometric parameter decreases. The buckling behavior of the frictional end with small friction coefficients presents an obvious difference compared to the results of high coefficients. For certain geometric parameters, the buckling mode of the spherical shell is transited because of changing the friction coefficient. A buckling map that describes the dependence of critical pressure on both friction coefficient and geometric parameter combined with buckling mode is generated. This map can be applied to the design of the spherical shell against buckling.

1. Introduction

Spherical shells have been widely used in a variety of applications from marine industries to aerospace because of their geometry, which is considered an ideal structure owning high pressure-supporting capacity [1–3]. The loss of stability in these shells may cause severe failures and has received great attention. The buckling of elastic thin spherical shells subjected to uniform external pressure is a well-known problem. Zoelly [4] first solved the critical buckling pressure based

✉ Yoshio ARAI, e-mail: yarai@mail.saitama-u.ac.jp

¹Saitama University, Saitama, Japan

²Hanoi University of Civil Engineering, Hanoi, Vietnam

³Tokyo Institute of Technology, Tokyo, Japan



on linear buckling shell theory and applied it to fully perfect spherical shells. Its equation is:

$$p_0 = \frac{2E}{\sqrt{3(1-\nu^2)}} \left(\frac{t}{R} \right), \quad (1)$$

where t is the thickness, and R is the radius; E and ν are Young's modulus and Poisson's ratio, respectively. Later, the nonlinear theory for large deformation was examined to determine the critical pressure and deformation of complete spherical shells and hemispheres by solving a system of four first-order differential equations of the shell theory where shooting and parallel shooting methods were used to obtain the numerical solutions [5] or to compare with the experimental results [6].

Many researchers have gained deep insight into the pre-buckling and post-buckling behavior of hemispherical shells and shallow spherical shells with the clamped end as a boundary condition under uniform external pressure, using experimental, analytical, and numerical methods. Von Kármán, and Tsien [7] presented a new theory of the mechanism of the collapse of spherical shells based on the minimum energy criteria. Then, the critical pressure and buckling deformation of shallow spherical shells were examined by using perturbation methods [8], power series calculations [9–11], and linearization [12]. To investigate the pressure-deflection curve and buckling characteristics of spherical caps, Keller and Reiss [13] introduced finite differences by employing an iteration procedure. Budiansky [14] exploited an integral-equation formulation to improve the accuracy of axisymmetric buckling pressure for all thicknesses of the spherical shell by numerical method. The numerical solutions were also achieved by solving the linear nonhomogeneous variational equations for the nonlinear system of equations [15] or by an assumption of the initiation of unsymmetrical deflection [16, 17]. Holston [18] presented an approximate analytical solution of the finite-deflection equations by Newton's method. Their results were in agreement with the known buckling results. Recently, with the power of the finite element method, the buckling behavior of shallow spherical shells with different boundary conditions and initial conditions was studied [1, 19–23].

Most studies have focused on the rigidly clamped edge as the boundary condition for shallow spherical shells. However, other boundary conditions at the end edge (i.e., hinged end) also influence the buckling strength of these shells. Pan and Cui [2] conducted an overview of the buckling and ultimate strength of a spherical pressure hull under external pressure, taking into consideration the effect of the end edge. They found that the critical pressure is affected by the type of end edge, whether it is rigidly clamped, simply supported, or elastically supported. Kai-Yuan, et al. [24] studied the axisymmetric buckling problem of thin, shallow, circular spherical shells under uniform external pressure with the end edge either rigidly clamped or simply supported and concluded that the buckling mode and critical pressure were significantly affected by the end edge boundary conditions. The edge conditions: clamped, simple, roller, or elastic support of shallow spheri-

cal shells were examined by Silverman and Mays [25] and showed a considerable difference in load-deflection curves. The buckling pressure of spherical caps also showed a considerable difference between clamped edge and simple support [26].

The effect of geometry on the critical buckling pressure of a thin shallow spherical shell under uniform external pressure with clamped or hinged ends has also been studied. Kaplan and Fung [8] tested the shallow spherical shell under oil and air pressures to obtain the critical pressure and compared it with theoretical values. The experiments were conducted for small values of the geometric parameter. The results showed that the critical pressure nonlinearly increases with the geometric parameter. These experimental critical pressures were used to compare with theoretical values [11, 12], numerical results [10, 13, 15, 16], and finite element results [1], and they showed good agreement in this range of the geometric parameter. For larger values of the geometric parameter, as the geometric parameter increases, the critical pressure also increases until it reaches a peak, and then it decreases [10–12, 15]. For very large values of the geometric parameter, the critical pressure remains unchanged as the geometric parameter increases [24].

Many authors have found a discrepancy between theoretically calculated and experimentally obtained critical buckling pressures. The theoretical values are typically three to four times higher than the experimental results [3, 7]. In order to explain this discrepancy, the presence of initial imperfections must be taken into account [6, 14–16, 27]. It is clear that both the shape and amplitude of initial geometric imperfections can influence the buckling behavior of spherical shells [2]. Numerical simulations by Zhou, et al. [20] have indicated that the critical buckling load decreases as the amplitude of imperfections increases. The effect of the initial geometric imperfection has also been analyzed through experiments, finite element modeling, and numerical solutions [28]. However, determining the real initial imperfection of the spherical shell is difficult. Therefore, the shape and size of the initial geometric imperfection of spherical shells are often introduced by using a linear buckling mode [20, 23, 29] or a dimple-like imperfection by force [21, 22].

Relating to the presence of friction in buckling problems of shallow spherical shells, the common objective, which is the collapse behavior of the spherical shells compressed by a rigid plate or between a rigid plate and an indenter, has been investigated. The frictional contact between the spherical shell and rigid support was often considered to have an unchanged coefficient [30–32], stick contact, or frictionless (perfect slip condition) [28, 33–35]. Most research showed that the friction between the shell and the plate surface plays an essential role in the buckling response and load-bearing capacity of the shell. Etsion and his team [36–41] studied the effect of contact conditions on the elasticity terminus of a deformable sphere compressed by a rigid flat, relying on experimental, theoretical, and numerical studies. The results indicated a considerable difference in critical values of load, interference, contact area, and contact pressure, as well as the location where the limit of elasticity was first reached due to the contact conditions with various material properties and spherical shell geometries. By changing the

coefficients of friction of the shell–indenter contact, Gupta [42] and Nasto, et al. [43, 44] concluded that friction has a dramatic effect on the mechanical response, load-bearing capacity, and deformed shape of the spherical shells. The critical buckling pressure with consideration of friction is considerably overestimated by a linear buckling analysis. Linear perturbation is often used to find the buckling shape for the introduction of the initial imperfection [28, 31, 45]. Moreover, linear buckling analysis is linear, while contact problems are nonlinear [46, 47]. Therefore, in contact problems without considering the initial imperfection, linear buckling analysis is often neglected.

It is worth noting that the majority of theories explaining the buckling behavior of spherical shells employ axisymmetric deformations [7, 9, 12, 14, 18]. Theoretical equations considering axisymmetric buckling have been established and solved using numerical methods [5, 10, 11, 15, 24, 26]. The buckling results of spherical shells subjected to uniform external pressures with a clamped end have also been obtained using axisymmetric modeling [10, 48]. Besides, when considering asymmetric buckling, both theoretical [49] and numerical results [16, 17] of spherical shells have been examined. Experiments have also observed that spherical shells can buckle asymmetrically [50, 51]. It should be noted that the presumed sources of the discrepancy between theoretical and experimental results are the asymmetric buckling [16, 17, 51]. In the case of buckling deformation with consideration of friction, axisymmetric buckling analyses [33] and axisymmetric finite element models [28, 39–42] were employed to examine the buckling behavior of spherical shells.

Most studies have focused on the buckling problems of shallow spherical shells under uniform external pressure with clamped end or hemispheres compressed by a rigid plate or an indenter with consideration of a given friction coefficient between them. Until now, there have been no studies on the buckling behavior of shallow spherical shells that take into account the effect of friction at the end edge. Starting from the motivation to add one more case of the end edge boundary condition of shallow spherical shells, this study investigates the buckling behavior of thin, shallow, elastic spherical shells under uniform external pressure with frictional contact between the end edge and rigid walls. Furthermore, the clamped end boundary condition of these shells is often created by different types of joining, such as adhesives [52], screws [48], bolts [8], and welds [29], which can ensure only a nearly fixed constraint [23]. Hence, these joining methods may be replaced by a proper friction coefficient. Therefore, it is necessary to consider the effect of friction at the end edge of shallow spherical shells on their buckling performance.

2. Methodology

To show how the friction at the edge contacting with the rigid walls influences the buckling behavior under uniform external pressure, a nonlinear buckling analysis has been carried out by using the finite element method.

2.1. Geometry and material properties

A schematic of the shallow spherical shell is shown in Fig. 1. The shell has a thickness t of 0.05 mm and a radius of curvature R of 77.70 mm. A rounded edge with a radius R_e of $1 \cdot 10^{-3}$ mm is created at the contact regions between the shell and rigid walls to avoid concentrated stresses.

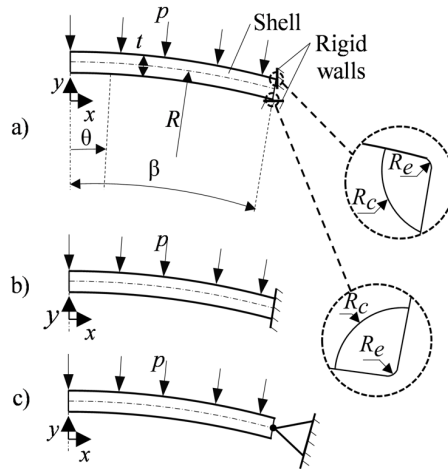


Fig. 1. The geometry of the shallow spherical shell, a) frictional end, b) clamped end, c) hinged end

Fig. 1 also illustrates the boundary conditions for the simulation, where the spherical shell is subjected to uniform external pressure p at the outer surface. The end edge of the shell is constrained with three different types of boundary conditions: frictional end, clamped end, and hinged end, shown in Fig. 1a, Fig. 1b, and Fig. 1c, respectively. In the frictional end, the end edge of the shell is supported by rigid walls, and a range of friction coefficient f is incorporated into the contacting areas to investigate its effect on the buckling behavior of the shell. The range of the friction coefficient examined is from $f = 0.0$ (frictionless) to $f = 4.0$ for each geometric parameter and is applied to the model by penalty formulation.

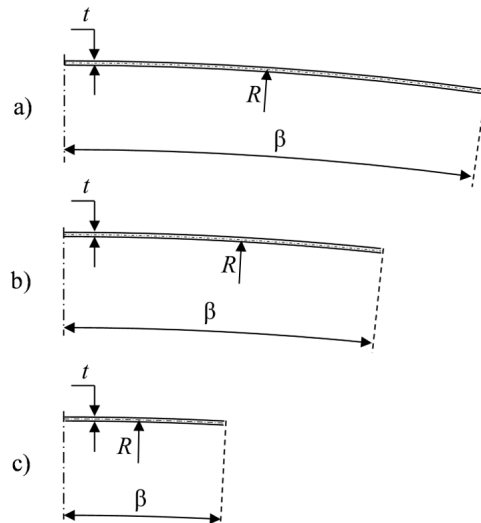
$$\rho = \left[6(1 - \nu^2) \right]^{\frac{1}{2}} \left(\frac{\beta^2 R}{t} \right). \quad (2)$$

A geometric parameter, ρ , defined according to Eq. (2), is considered a variable parameter, where β is the semi-angle of the shell opening. In this analysis, nine different geometric parameters are taken as 8.6, 9.9, 18.4, 22.2, 27.4, 32.4, 36.8, 53.6, and 71.8.

A configuration of the shallow spherical shells for three different geometric parameters is shown in Fig. 2. The spherical shells used for this study are made of aluminum alloy AA6061-T6 and its mechanical properties are shown in Table 1. The shell is assumed as an isotropic, homogeneous, and elastic material.

Table 1. Mechanical properties of AA6061-T6

Young's modulus, E , MPa	Poisson's ratio, ν
68900	0.33


 Fig. 2. Configuration of the shallow spherical shells, a) $\rho = 71.8$, b) $\rho = 36.8$, and c) $\rho = 8.6$

2.2. Numerical model

In this study, an axisymmetric model is adopted due to the axisymmetric geometry of the structure under axisymmetric loading. This model has proven highly efficient in addressing buckling problems of spherical shells, whether considering friction or not, as indicated in the literature. Furthermore, the analysis of non-axisymmetric buckling behavior is notably challenging [49, 51], and requires substantial computational resources and time (nearly 20 times) [28, 51]. Hence, for the sake of simplification, this study employs the axisymmetric model to examine the buckling behavior of spherical shells. A four-node axisymmetric quadrilateral element (CAX4R) with reduced integration and hourglass control is employed for the analysis to reduce the computation time and enhance convergence. In this simulation, the spherical shell is regarded as a constant radius, and the thickness is also unchanged and uniform. As previously mentioned, the determination of the actual shape and size of the initial imperfection is challenging. Moreover, when the amplitude of the initial imperfection is below 1% of the shell thickness, shells are generally assumed to be almost perfect [53, 54]. Therefore, the effect of the initial imperfection is not taken into account in this study.

The buckling results of the frictional end are compared with those of the clamped and hinged ends. The rigid walls in the frictional end are considered fixed. In the clamped end, all degrees of freedom of the end edge of the shell are constrained, while in the hinged end, only the center of the end edge is restrained from displacements, allowing its end edge to rotate freely.

2.3. Analytical process

The mesh size has an essential effect on the accuracy of numerical simulation results. A finite element model, however, with a very fine mesh may increase the computational time and cost. For this reason, at the initial step of this simulation, a mesh convergence analysis is carried out by varying the number of elements to choose an appropriate mesh. The total number of elements N and the number of elements along the thickness N_t corresponding to twelve different mesh sizes presented in Table 2 are examined for one case of the geometric parameter ρ of 9.9, and the critical buckling pressure is compared.

Table 2. The number of elements along the thickness and number of elements corresponding to different mesh sizes

Mesh size, 10^{-3} mm	25	12.5	8.3	6.3	5.0	4.2
N_t	2	4	6	8	10	12
N	326	1304	2940	5208	8140	11628
Mesh size, 10^{-3} mm	3.6	3.2	2.8	2.5	2.0	1.7
N_t	14	16	18	20	25	30
N	15820	20256	26154	32560	50875	73080

It is necessary to create a finer mesh density near the contact regions between the shell and rigid walls in the frictional end [39–41]. Therefore, a mesh size of $0.08 \cdot 10^{-3}$ mm surrounding the contact zone by a radius R_c of 0.01 mm is generated as shown in Fig. 3. The mesh density is gradually increased to ensure that the closer the contact regions, the finer the mesh size is assigned. The intersection curves between coarse and fine mesh regions have meshed with the same number of elements to ensure the continuity of the elements. This mesh modeling of the contact regions is applied equally to all configurations of the spherical shell.

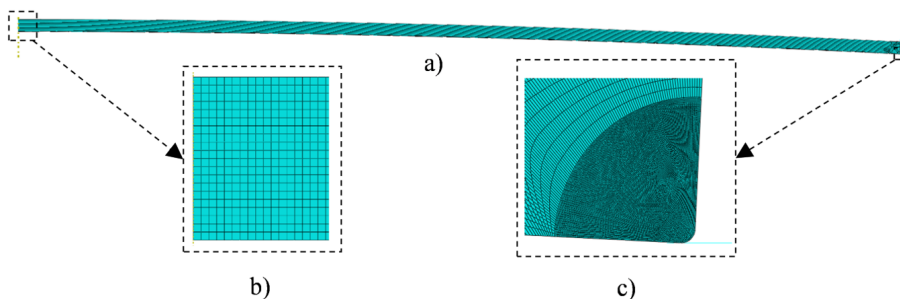


Fig. 3. A sample of mesh ($\rho = 9.9$), a) overall mesh, b) center part, c) contact zone

To reduce the effect of the aspect ratio of the element, the size of the element along the thickness and the longitudinal direction are divided equally.

Both the mesh refinement step and nonlinear buckling analysis in this study used the Riks algorithm [55–57] to trace the pressure-displacement curve. This algorithm can accurately predict the critical pressure and buckling deformation of the spherical shells [20–23] or hemispherical shells compressed by a rigid plate with frictional contact [28, 31, 44]. In this analysis, geometry nonlinearity is taken into consideration.

The critical pressure is normalized with one of the fully perfect spherical shells, known as the relative critical pressure p_{cr}/p_0 . The relationship between relative critical pressure and the total number of elements is shown in Fig. 4. It can be seen that the mesh size has a significant influence on the critical buckling pressure of the spherical shell. A coarse mesh corresponding to a small number of elements will decrease the critical pressure. The results are nearly unchanged when the mesh density reaches a certain value [20, 58]. Thus, a mesh density of $2.5 \cdot 10^{-3}$ mm with 32 560 elements is considered a proper mesh for this analysis [22, 28, 58]. An illustration of the chosen mesh at the center part and the contact zone is displayed in Fig. 3 as an example.

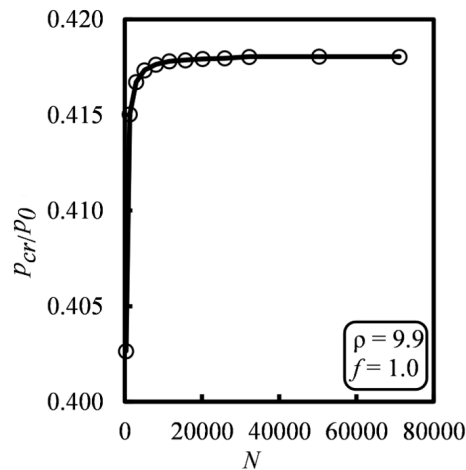


Fig. 4. Relationship between the relative critical pressure and the total number of elements

3. Result and discussion

The critical buckling pressure of the clamped end for different geometric parameters has been obtained and compared with previous studies. It can be observed in Fig. 5 that there is a peak in the buckling pressure when the geometric parameter increases. The experiment [8] also presents a peak of the critical buckling pressure. However, experimental results show lower critical pressures due to the initial

imperfection and irregularity of the shell, while the numerical [11, 24], the finite element results [1], and the present results are in good agreement.

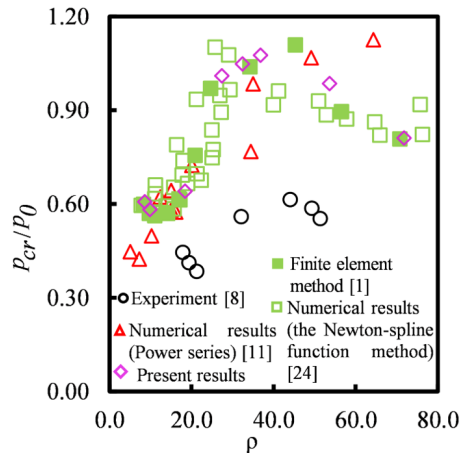


Fig. 5. Plot of relative critical pressure versus geometric parameter for the clamped end

To examine the effect of friction on the buckling behavior of the shell, equilibrium paths presenting the uniform external pressure plotted against the displacement at the center w_c , are shown in Fig. 6 for the clamped, hinged, and frictional ends. Four geometric parameters representing different buckling modes and mode transitions are selected to capture the results. The circle points indicate the critical points at which the pressure reaches a peak, and the shell loses its stability. In general, increasing the coefficient of friction causes the equilibrium path of the frictional end to converge with the clamped end. In the case of the geometric parameter ρ of 18.4 as presented in Fig. 6b, a high critical pressure, which is even higher than the one of the clamped end, can be seen in a range of the friction coefficient from over 1.0 to 2.0. This greater tendency will be explained based on the buckling mode of the shell later. For each geometric parameter, the equilibrium path of small friction coefficients ($f < 1.0$) has the same type and shows a clearer difference than those of high friction coefficients. For all geometric parameters, the shell experiences a large displacement at the center when the coefficient of friction is small at the same pressure in the pre-buckling stage. In other words, the frictionless end undergoes the greatest deflection, which gradually decreases in magnitude with the increase of friction coefficient under the same external pressure. The higher the friction coefficient, the harder the shell deforms. Although the end edge of the hinge end can rotate freely, it shows a smaller magnitude of displacement at the center than the frictionless end before the shell buckles, regardless of the geometric parameter. The small geometric parameter ($\rho = 8.6$) in Fig. 6a and the large geometric parameter ($\rho = 71.8$) in Fig. 6d present a monotonic increase in displacement as the pressure increases. This same tendency can be seen in the medium geometric parameter ($\rho = 18.4$ and $\rho = 36.8$) at low friction

coefficients ($f < 1.0$) in Fig. 6b and Fig. 6c. However, at high friction coefficients of the medium geometric parameter as shown in Fig. 6c, the displacement initially increases and then decreases when the pressure increases.

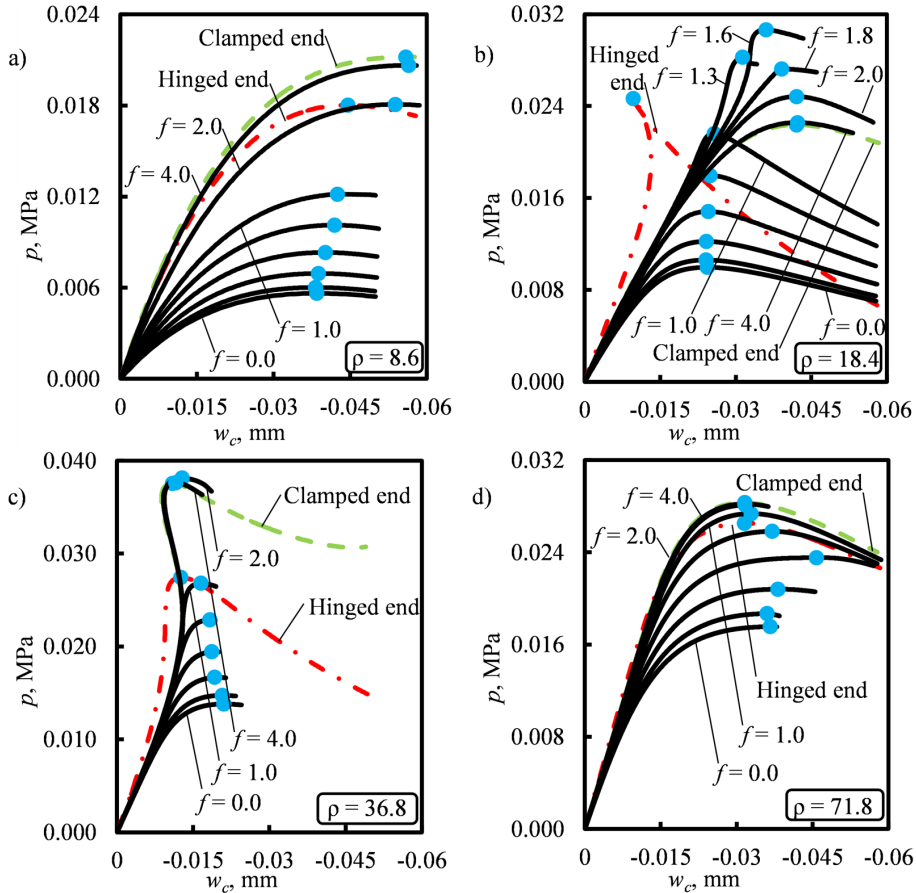


Fig. 6. Equilibrium path for different geometric parameters with clamped, hinged, and frictional ends of boundary condition

To observe the deformation of the spherical shell during the pre-buckling stage, a distribution of displacement w along the polar angle θ at different pressure values is illustrated in Fig. 7. As shown in Fig. 7a, b, and c, three distinct geometric parameters corresponding to three types of buckling modes with the same friction coefficient are considered to show the deformation. Firstly, the mode of deformation should be defined for discussion. The mode of deformation indicates the number of extreme points of the displacement distribution and the locations of these points along the polar angle of the spherical shell. Mode of deformation I (mode I) has only one extreme point located at the center of the shell. Likewise, mode of deformation II (mode II) shows two extrema, one at the center and the other at the

place between the center and the edge, and mode of deformation III (mode III) has three distinct peaks of displacement, one at the center and two remaining points occurring between the center and the edge [10–12, 24]. At the smallest geometric parameter in Fig. 7a, as well as at the critical pressure of the equilibrium path in Fig. 6a with the friction coefficient $f = 2.0$, the shell buckles in mode I; before that, only the mode of deformation I occurs. With a wider opening angle in Fig. 7b, when the pressure increases, it first witnesses the mode of deformation I and then changes to buckling mode II before the critical pressure indicated in Fig. 6c with $f = 2.0$. Similarly, at the highest geometric parameter in Fig. 7c, both modes of deformation I and II are observed before the shell buckles in mode III at critical pressure shown in Fig. 6d with $f = 2.0$. It can be observed in Fig. 7b and Fig. 7c that when the buckling mode changes from mode I to mode II, a new local maximum displacement occurs between the center and the old local maximum. By the same principle, the transition from mode II to mode III creates a new local minimum at the center, and the peaks in mode II move closer to the end edge of the shell in mode III. The transition of the buckling mode, in essence, generates a new extreme point of displacement at the center and yields a new quarter waveform along the polar angle of the shell. When the pressure increases, the transition of the mode of deformation from mode I to mode II causes a decrease in displacement magnitude at the center region, as shown in Fig. 7b. The effect of friction on the distribution of displacement at the same geometric parameter is also examined in Fig. 7b, d, and e. In these figures, a decrease in the friction coefficient causes the decrease phenomenon in displacement at the center region to disappear, even though the transition of the mode of deformation still occurs. Additionally, a change in the friction coefficient leads to a change in the buckling mode from mode II at $f = 2.0$, as shown in Fig. 7b, to the onset of mode III in the frictionless end, as indicated in Fig. 7e. At this point, the onset of mode III is marked by a minimum displacement at the center and two distinct peaks situated between the center and the edge as presented by circle points in Fig. 7e. As shown in Fig. 7f, there is a minimum displacement at the center and a maximum point located nearby.

The distribution of vertical displacement at the critical pressure along the polar angle of the spherical shell for different geometric parameters with three types of boundary conditions is presented in Fig. 8 to investigate the effect of friction on the buckling mode of the spherical shell. As illustrated in Fig. 8a, the spherical shell with the smallest geometric parameter is buckled in the mode of deformation I. As the shell opening angle increases, the buckling mode transits to mode II and then mode III in a sequence. A transition phenomenon of the buckling mode of the spherical shell under the same geometric parameters from mode I to mode II and from mode II to mode III due to a decrease in friction has also been observed in Fig. 8b and Fig. 8c, respectively. As depicted in Fig. 8b, when the frictional end has a coefficient over 2.0, and the end edge is clamped, mode I of buckling occurs. When the friction coefficient decreases, the buckling mode changes to mode II, the same as the hinged end. When the friction coefficient decreases from 2.0 to 1.0, the

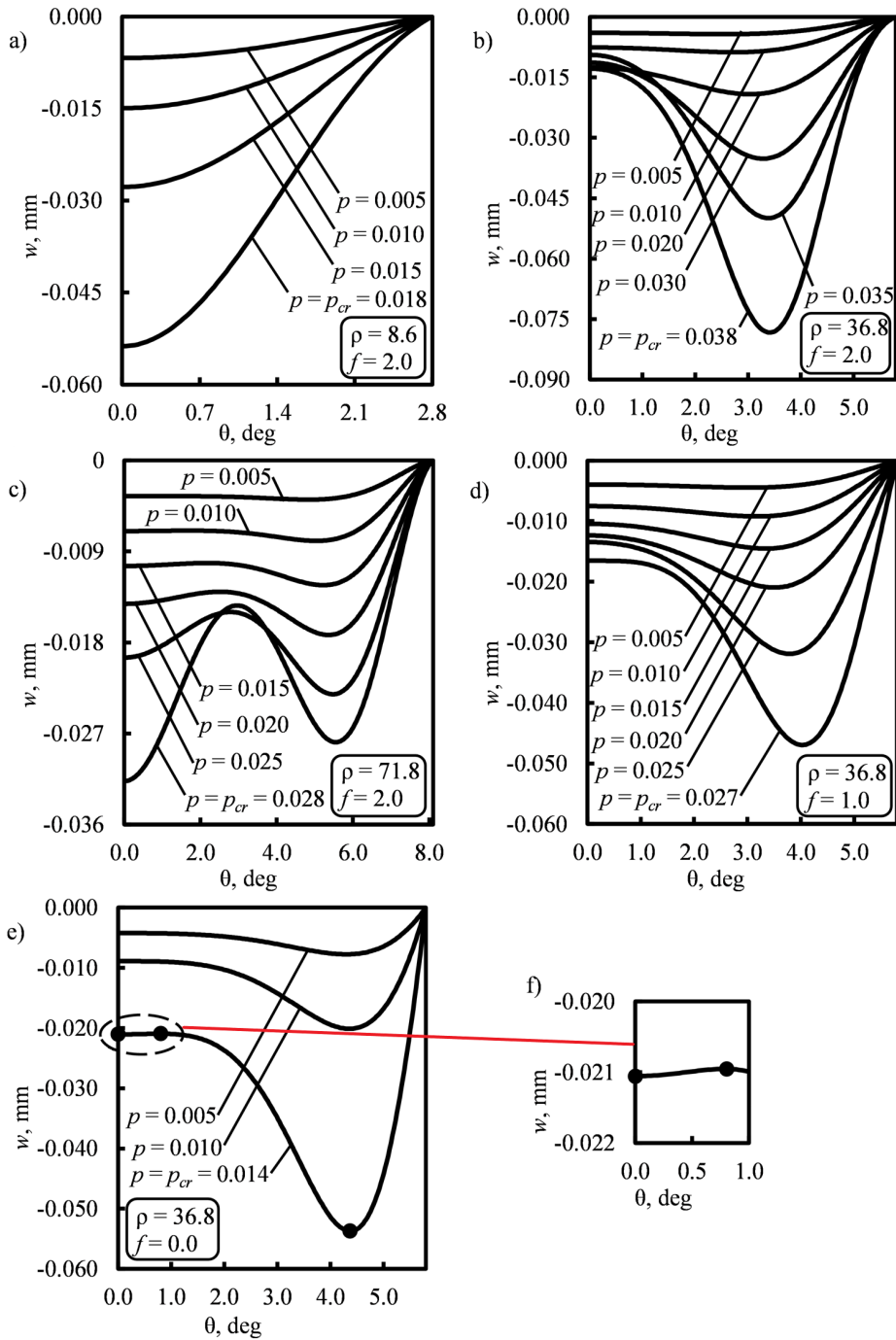


Fig. 7. Distribution of displacement along the polar angle during the pre-buckling stage for different geometric parameters at the same friction coefficient and for different friction coefficients at the same geometric parameter

buckling mode transition occurs, and the critical pressure becomes higher at this range of friction coefficient, as shown in Fig. 6b. Similarly, the change of buckling mode from mode II to mode III in Fig. 8c occurs when the friction coefficient decreases as shown in Fig. 8b. The transition of the buckling mode under the same opening angle reveals the effect of friction on the buckling mode of the spherical shell. It should be noted that for all geometric parameters in Fig. 8, the distribution of displacement in the frictional end with a high friction coefficient converges to that of the clamped end. The hinged and frictionless ends always exhibit the same buckling mode, regardless of the geometric parameter.

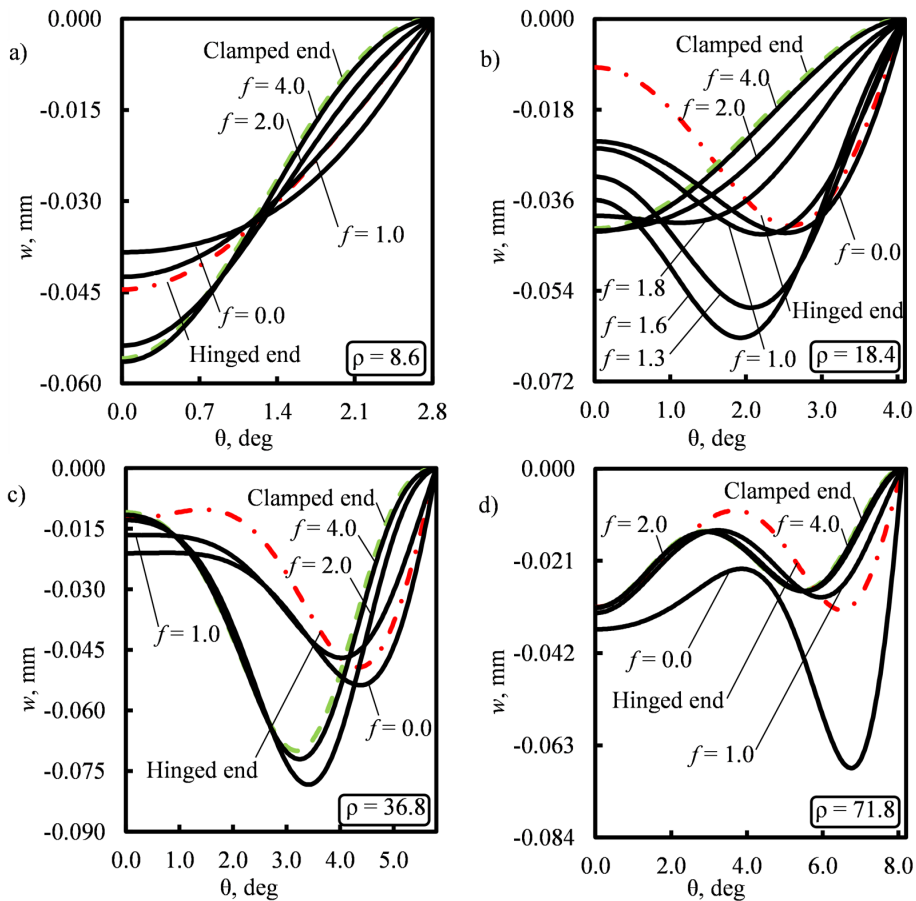


Fig. 8. Distribution of vertical displacement along the polar angle at critical pressure for different geometric parameters with different boundary conditions

From the equilibrium paths as shown in Fig. 6, critical pressures are extracted and plotted against the friction coefficient in Fig. 9a and the geometric parameter in Fig. 9b. The results of the frictional end with different coefficients are compared with those of the clamped and hinged ends. As shown in Fig. 9a, for small friction

coefficient values ($0.0 \leq f \leq 1.6$), the critical pressure increases nonlinearly with a considerable change when the friction coefficient increases. In the high range of the friction coefficient ($1.6 < f \leq 4.0$), there is a slight change in the critical buckling pressure, which then converges with one of the clamped end.

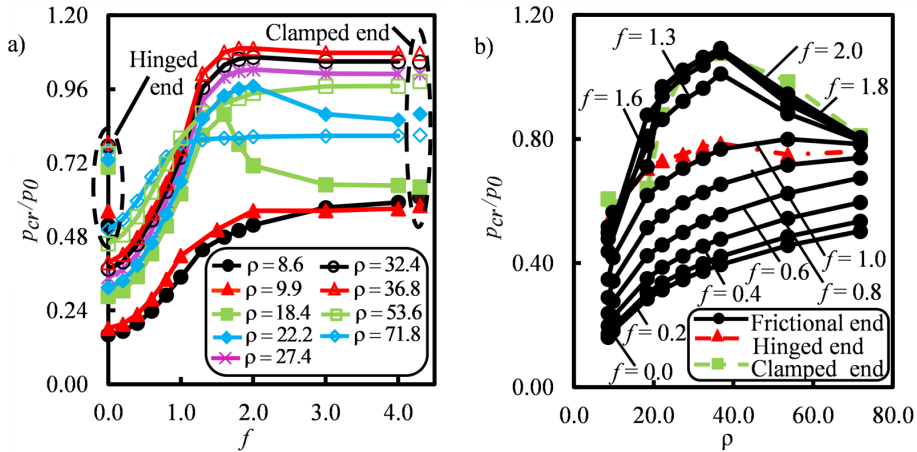


Fig. 9. a) The relationship between the relative critical pressure and friction coefficient for different geometric parameters with three types of boundary condition, b) The relationship between the relative critical pressure and geometric parameter with different boundary conditions

It can be seen from Fig. 9a and Fig. 9b that the critical pressure for the frictionless end is extremely low compared to other ends of boundary conditions. The critical pressure of the hinged end is 1.5 to 3.2 times higher than that of the frictionless end. The dependence of the relative critical pressure on the geometric parameter is shown in Fig. 9b. For a small range of friction coefficient ($0.0 \leq f \leq 1.0$), the critical pressure increases nonlinearly with an increase in the geometric parameter. A wider spherical shell presents a greater critical pressure, making it more resistant to buckling [59]. Due to the convergence of the frictional end at high friction coefficients with the clamped end, the critical pressure at high coefficients fluctuates and peaks at the same value of the geometric parameter as the clamped end, frictionless end. Considering the stability curves in Fig. 6, under the same pressure during the pre-buckling stage, the spherical shell in the frictionless end suffers the largest displacement in magnitude at the center, regardless of the geometric parameter. It points out that without friction, the spherical shell is easier to deform under external pressure.

Components of the reaction force at the top and bottom corners and the angle of rotation of the end edge φ are illustrated in Fig. 10. Because the length of the contact regions is relatively small compared to the thickness of the spherical shell, these reaction forces are considered concentrated forces. The angle of rotation represents the degree of rotation from the initial state of the end edge of the shell.

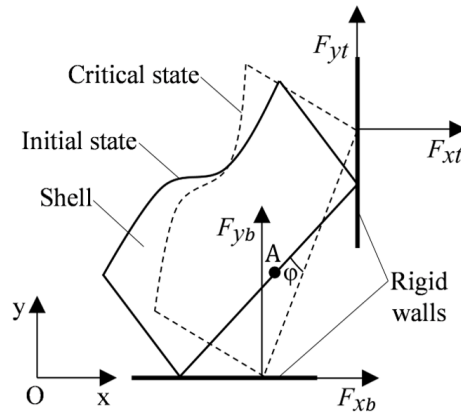


Fig. 10. Illustration of the angle of rotation and reaction forces

Fig. 11a, b, c, and d show the reaction force in the horizontal direction F_{xt} and the vertical direction F_{yt} at the top corner, and in the horizontal direction F_{xb} and the vertical direction F_{yb} at the bottom corner for a specific geometric parameter at different values of the friction coefficient, respectively. It can be seen from Fig. 11a and c that at the same pressure as the critical pressure of the frictionless end, the horizontal reaction force at the top corner exhibits a significant value, as this reaction force at the bottom corner, regarded as the frictional force, is zero. Therefore, the high horizontal reaction force at the top corner is responsible for maintaining the balance. Under the same external pressure, as the friction coefficient increases, the horizontal reaction force at the bottom corner also increases, leading to a decrease in the horizontal reaction force at the top corner.

The vertical reaction forces at the top and bottom corners are presented in Fig. 11b and c. At the top corner, the vertical reaction force is negative, while at the bottom corner, it is positive. The contrasting relationship between the horizontal reaction force at the top corner and the friction coefficient, under the same external pressure, results in a fluctuation of the vertical reaction force at the top corner. Due to the principle of equilibrium, the sum of the vertical reaction forces at the top and bottom corners remains constant. Consequently, the vertical reaction force at the bottom corner also exhibits fluctuations, corresponding to the changes in the friction coefficient.

The resultant moment of force M due to the reaction forces at the top and bottom corners at the critical pressure is shown in Fig. 12. This resultant moment of force is calculated at the center point of the end edge (point A in Fig. 10). In cases of the frictional end, the resultant moment of force corresponds to the bending moment at the end edge of the spherical shells. It has a positive value in the anticlockwise direction, and vice versa. At small friction coefficients, the resultant moment of force is anticlockwise, aligning with the direction of the angle of rotation of the end edge. However, at high friction coefficients, it decreases and

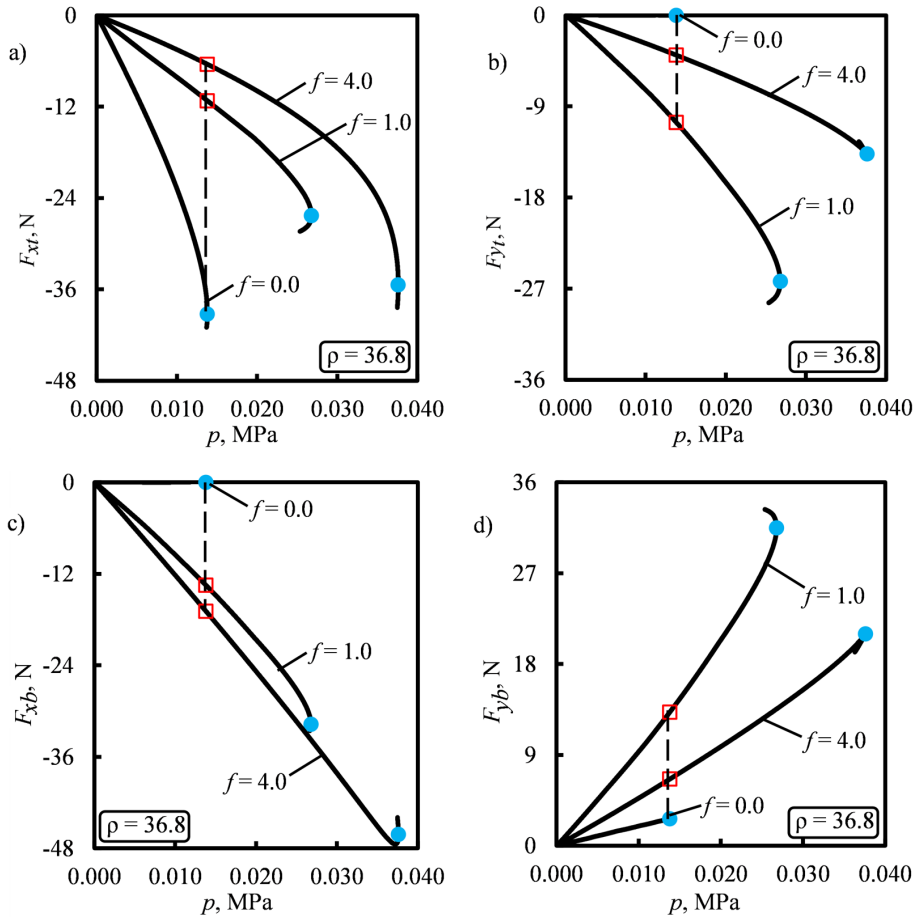


Fig. 11. a) Horizontal reaction force, b) vertical reaction force at the top corner, and c) horizontal reaction force, d) vertical reaction force at the bottom corner for a specific geometric parameter with different friction coefficients

changes to the clockwise direction, opposing the direction of the rotation angle of the end edge.

The angle of rotation of the end edge at the same pressure as the critical pressure of the frictionless end and at critical pressure for different geometric parameters are shown in Fig. 13a and b, respectively. Positive values of the angle of rotation indicate that the end edge rotates in the anticlockwise direction. For all geometric parameters, the rotation angle of the end edge of a shallow spherical shell under the same pressure shows the smallest value at a higher value of friction coefficient as shown in Fig. 13a. As the friction coefficient decreases, this angle of rotation monotonically increases. Higher friction coefficients make the shallow spherical shell harder to rotate. Fig. 13a also demonstrates that in the frictional end, the angle of rotation decreases as the geometric parameter increases. In other words,

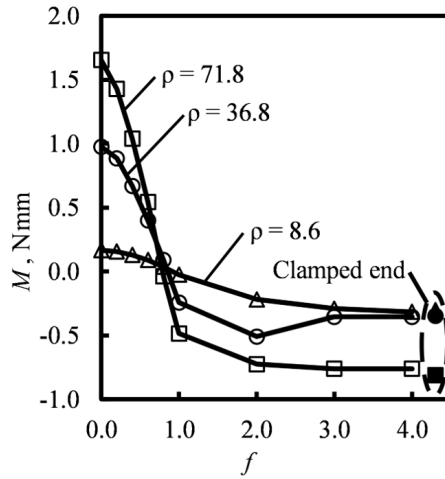


Fig. 12. Resultant moment of force at the critical pressure for different geometric parameters

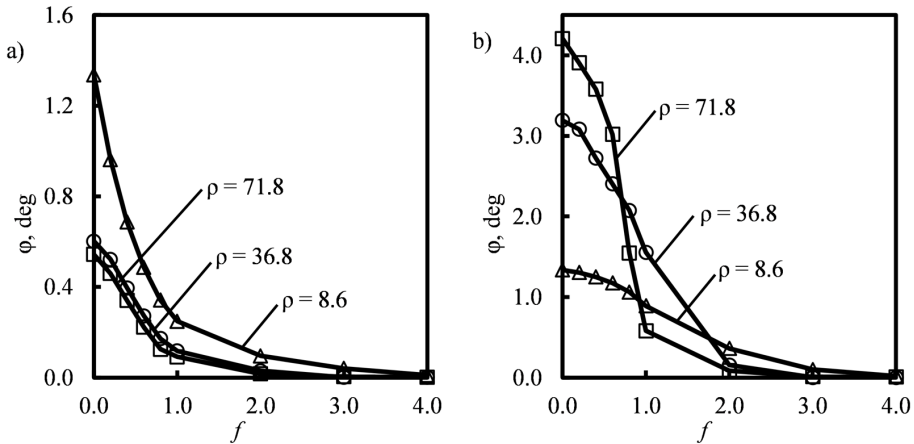


Fig. 13. The angle of rotation of the end edge a) at the same pressure as the critical pressure of the frictionless end, and b) at critical pressure for different geometric parameters

a narrow spherical shell is easier to rotate than a wider one under external pressure. The rotation of the end edge of shallow spherical shells at the critical pressure is always in the anticlockwise direction as depicted in Fig. 13b. As the friction coefficient decreases, the rotation angle of the end edge increases, regardless of the geometric parameter. The spherical shell is less prone to rotation with higher friction coefficients.

The hinged end has no moment of force at the end edge, while the frictionless end exhibits an anticlockwise moment of force (as indicated in Fig. 12) due to the presence of a couple of reaction forces at the top and bottom corners. The direction of this moment of force in the frictionless end aligns with the angle of

rotation of the end edge as shown in Fig. 13b, while this direction is opposite in the clamped end. This moment of force could explain the smaller critical pressure in the frictionless end compared to that in the hinged end.

Fig. 14a, c and Fig. 14b, d show the tangential stress distribution σ_t at the pressure the same as the critical pressure of the frictionless end and at the critical pressure, respectively. In these figures, the distribution of tangential stress at the inner and outer surfaces of the shell with different geometric parameters at distinct friction coefficients is considered. As shown in Fig. 14a and c, at the pressure equal to the critical pressure of the frictionless end, the bending stress without friction is greater than that considering friction at different geometric parameters. This small bending stress in the frictional end explains the reason why the shell does not buckle at the same pressure as the critical buckling pressure of the frictionless end. The bending stress near the end edge shows a difference in sign between with

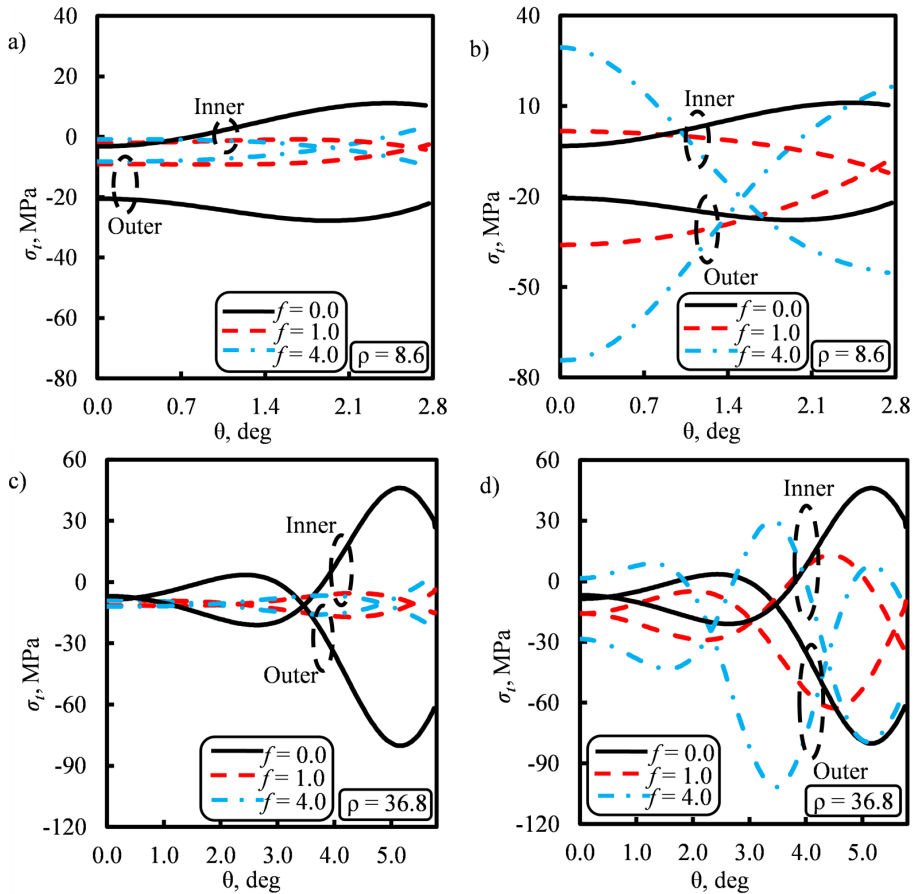


Fig. 14. Distribution of tangential stress for different geometric parameters with different friction coefficients, a, and c) at the same pressure as the critical pressure of the frictionless end, b, and d) at the critical pressure

and without friction. This change in sign is due to the high horizontal reaction force at the top corner in the case of the frictionless end, as mentioned before in Fig. 11. As indicated in Fig. 14a and c, a change of bending stress generates a point where there is no bending stress (the point at which the stress at the inner and outer surfaces is the same). When the pressure reaches the critical pressure in the frictional end, as illustrated in Fig. 14b and d, the magnitude of the bending stress increases, regardless of the geometric parameter and friction coefficient.

The dotted arrows in Fig. 15 depict the movement of the no-bending points for a specific geometric parameter within a small range of friction coefficient ($0.8 \leq f \leq 1.3$), during which a transition in the buckling mode from mode III to mode II as the friction coefficient increases. The central portion of Fig. 15a is highlighted in Fig. 15b. As the friction coefficient increases, the moment of force due to the reaction forces changes its direction, as demonstrated in Fig. 13b. In other words, the bending moment at the end edge of the shell reverses its sign. Consequently, a new no-bending point emerges near the end edge, as depicted in Fig. 14b, d, and Fig. 15a. With the friction coefficient continuously rising, the magnitude of the bending moment at the end edge also grows. This increase leads to the shifting of not only the newly formed no-bending point but also the pre-existing ones, all closer to the center. In certain specific geometric cases, such as the one represented in Fig. 15 ($\rho = 36.8$), the no-bending point near the center reaches the center as the friction coefficient increases from 0.8 to 1.0 as illustrated in Fig. 15b and then the bending moment at the center no longer equals zero as friction coefficient is larger than 1.0. Consequently, the number of no-bending points decreases, leading to a decrease in the buckling mode.

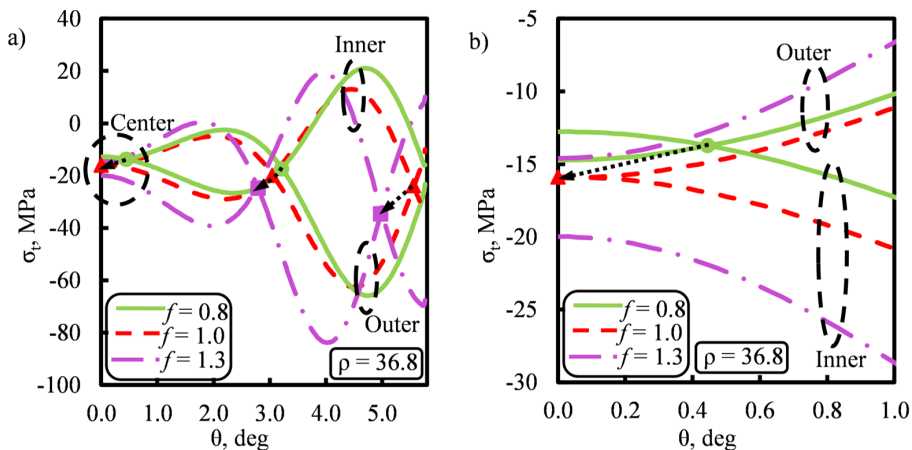


Fig. 15. Movement of the no-bending points

The distribution of displacement at the pressure equivalent to the critical pressure of the frictionless end is shown in Fig. 16. This figure considers different geometric parameters with varying friction coefficients. At any position of the

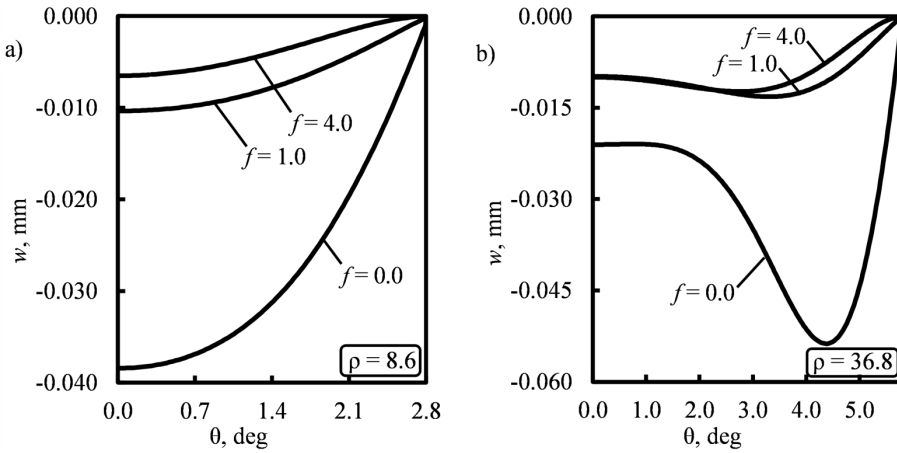


Fig. 16. Distribution of displacement for different geometric parameters with different friction coefficients at the same pressure as the critical pressure of the frictionless end

polar angle apart from the end edge, the larger the friction coefficient, the smaller the displacement value, regardless of the geometric parameter. This finding again indicates that the presence of friction makes the shell more difficult to displace. In the case without friction, the shell displaces more easily.

$$\frac{p_{cr}}{p_0}(f_{ref}, \rho_{ref}) = a_1 + a_2 f_{ref} + a_3 \rho_{ref} + a_4 f_{ref}^2 + a_5 f_{ref} \rho_{ref}, \quad (3)$$

where

$$f_{ref} = \frac{f - 1.632}{1.393} \quad (4)$$

and

$$\rho_{ref} = \frac{\rho - 31.79}{119.5}. \quad (5)$$

The relative critical pressure in Fig. 9 can be expressed as a function of the friction coefficient and geometric parameters. Therefore, a buckling map that describes the relationship between relative critical pressure and these parameters, combined with the mode of buckling, is illustrated in Fig. 17. To determine the contour plot of the relative critical pressure, the variation of relative critical pressure with respect to the friction coefficient and geometric parameter is presented in Eq. (3). The constants a_i ($i = 1, \dots, 18$) are determined using the linear least squares fitting method and are shown in Table 3.

From Eq. (3), the relative critical pressure can be predicted for each pair of friction coefficient and geometric parameters with a root mean squared error (RMSE) of 0.058. The relationships between relative critical pressure, geometric parameter, and friction coefficient in Fig. 17 agree well with these relationships as shown in Fig. 9. Specifically, when the geometric parameter and friction coefficient increase, the changes in relative critical pressure are the same in both figures.

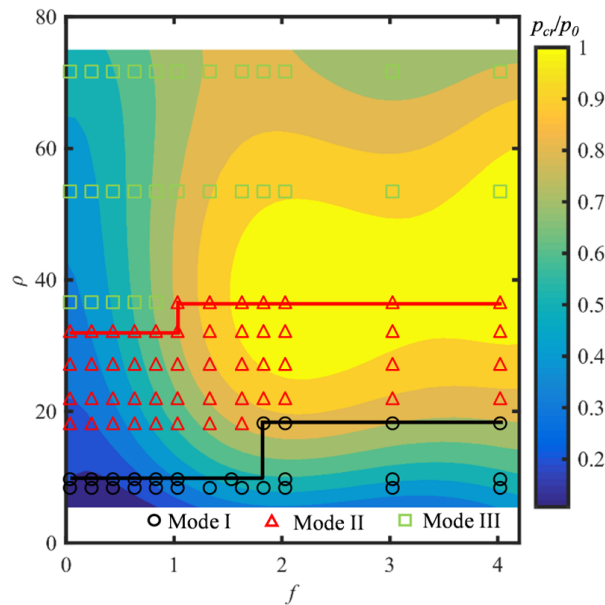


Fig. 17. Buckling map

Table 3. The constants of the fitted equation to determine the surface describing the relationship between relative critical pressure and friction coefficient and geometric parameter

a_1	a_2	a_3	a_4	a_5	a_6
0.987	0.314	0.108	-0.215	0.071	-0.325
a_7	a_8	a_9	a_{10}	a_{11}	a_{12}
0.036	0.003	-0.163	0.106	0.009	0.066
a_{13}	a_{14}	a_{15}	a_{16}	a_{17}	a_{18}
-0.050	0.079	-0.003	-0.022	0.041	-0.037

As shown in Fig. 17, the optimal shape of a spherical shell can be determined to obtain the greatest critical buckling pressure when applied to design problems. The highest critical pressure values occur when the geometric parameter is between 22.0 and almost 50.0, the friction coefficient is greater than 1.6. Using this buckling map, the buckling mode can be estimated for given values of the geometric parameter and friction coefficient, and the transition of the buckling mode can be determined simultaneously. The black and red lines indicate the boundary between buckling modes I and II, and buckling modes II and III, respectively. As demonstrated in Fig. 17, the buckling mode increases as the geometric parameter rises. For most geometric parameters, a decrease in the friction coefficient does not lead to any change in the buckling mode. However, at $\rho = 36.8$, the buckling mode transitions from mode II to mode III, and at $\rho = 18.4$, the buckling mode changes from mode I

to mode II Eq. (3) can be simplified as follows:

$$p_{cr} = K \frac{2E}{\sqrt{3(1-\nu^2)}} \left(\frac{t}{R}\right)^2. \quad (6)$$

Here, K is a coefficient describing the influence of the boundary conditions at the end edge on the critical pressure of the shallow spherical shell. The critical pressure at the clamped end is always greater than that at the hinged end [11, 17, 24, 26]. Therefore, the value of K at the clamped end is higher than its value at the hinged end. Similarly, in the frictional end, as the friction coefficient decreases, the value of K also decreases.

4. Conclusions

The buckling behavior of thin, shallow, elastic spherical shells under uniform external pressure with frictional, clamped, and hinged ends are examined using an axisymmetric finite element model. Nonlinear analysis is utilized to obtain buckling results for the frictional end with a wide range of friction coefficients, which are then compared to results for the two other ends. The following conclusions are found in this study:

- Friction has a strong effect on critical buckling pressure and displacement of the shell, especially at small values of friction coefficient. However, at high friction coefficients, the effect is less pronounced. In general, as the friction coefficient or geometric parameter decreases, the resistance of the shell to buckle also decreases. This occurs because, at small friction coefficients or geometric parameters, the spherical shell becomes more susceptible to rotating and displacing under uniform external pressure.
- The buckling mode is also influenced by friction. For specific geometric parameters, when the friction coefficient decreases, the mode of buckling changes from mode I to mode II and from mode II to mode III due to changes in the direction and magnitude of the moment of force at the end edge.
- A map of buckling describing the relationship of buckling mode, critical pressure, geometric parameter, and friction coefficient has been established.

This study employs an axisymmetric model to analyze the buckling behavior of spherical shells. It is assumed that the buckling deformation occurs in two dimensions, which may result in some variations compared to the actual three-dimensional characteristics of real-world structures. However, opting for a three-dimensional model introduces a high level of complexity. To simplify the analysis, the limitations of this model are acknowledged, and the non-axisymmetric buckling behavior of spherical shells is identified as a potential subject for further study.

Acknowledgements

This study was supported by the Ministry of Education, Science, Sports, and Culture of the Government of Japan.

References

- [1] J. Marcinowski. Stability of relatively deep segments of spherical shells loaded by external pressure. *Thin-Walled Structures*, 45(10–11):906–910, 2007. doi: [10.1016/j.tws.2007.08.034](https://doi.org/10.1016/j.tws.2007.08.034).
- [2] B. Pan and W. Cui. An overview of buckling and ultimate strength of spherical pressure hull under external pressure. *Marine Structures*, 23(3):227–240, 2010. doi: [10.1016/j.marstruc.2010.07.005](https://doi.org/10.1016/j.marstruc.2010.07.005).
- [3] J. Zhang, M. Zhang, W. Tang, W. Wang, and M. Wang. Buckling of spherical shells subjected to external pressure: A comparison of experimental and theoretical data. *Thin-Walled Structures*, 111:58–64, 2017. doi: [10.1016/j.tws.2016.11.012](https://doi.org/10.1016/j.tws.2016.11.012).
- [4] R. Zoelly. *About a Buckling Problem on the Spherical Shell* (Über ein Knickungsproblem an der Kugelschale). PhD Thesis, Zurich, 1915 (in German).
- [5] L. Bauer, E. L. Reiss, and H. B. Keller. Axisymmetric buckling of hollow spheres and hemispheres. *Communications on Pure and Applied Mathematics*, 23(4):529–568, 1970. doi: [10.1002/cpa.3160230402](https://doi.org/10.1002/cpa.3160230402).
- [6] L. Kollar. Buckling of complete spherical shells and spherical caps. In *Proceeding of a State-of-the-Art Colloquium*, pages 401–425, Berlin, Germany, 1982. doi: [10.1007/978-3-642-49334-8_14](https://doi.org/10.1007/978-3-642-49334-8_14).
- [7] T. Von Karman and H. Tsien. The Buckling of Spherical Shells by External Pressure. *Journal of the Aeronautical Sciences*, 7(2):43–50, 1939. doi: [10.2514/8.1019](https://doi.org/10.2514/8.1019).
- [8] A. Kaplan and Y.C. Fung. *A Nonlinear Theory of Bending and Buckling of Thin Elastic Shallow Spherical Shells*. NACA Technical Note 3212, pages 1–58, California Institute of Technology, Washington, 1954.
- [9] R.M. Simons. A power series solution of the nonlinear equations for axi-symmetrical bending of shallow spherical shells. *Journal of Mathematics and Physics*, 35(1–4):164–176, 1956. doi: [10.1002/sapm1956351164](https://doi.org/10.1002/sapm1956351164).
- [10] E.L. Reiss, H.J. Greenberg, and H.B. Keller. Nonlinear deflections of shallow spherical shells. *Journal of the Aeronautical Sciences*, 24(7):533–543, 1957. doi: [10.2514/8.3893](https://doi.org/10.2514/8.3893).
- [11] H.J. Weinitschke. On the nonlinear theory of shallow spherical shells. *Journal of the Society for Industrial and Applied Mathematics*, 6(3):209–232, 1958. doi: [10.1137/0106015](https://doi.org/10.1137/0106015).
- [12] E.L. Reiss. Axially symmetric buckling of shallow spherical shells under external pressure. *Journal of Applied Mechanics*, 25(4):556–560, 1958. doi: [10.1115/1.4011872](https://doi.org/10.1115/1.4011872).
- [13] H.B. Keller and E.L. Reiss. Spherical cap snapping. *Journal of the Aerospace Sciences*, 26(10):643–652, 1959. doi: [10.2514/8.8240](https://doi.org/10.2514/8.8240).
- [14] B. Budiansky. *Buckling of Clamped Shallow Spherical Shells*. Technical Report No. 5, pages 1–48, Harvard University, Massachusetts, 1959.
- [15] G.A. Thurston. A numerical solution of the nonlinear equations for axisymmetric bending of shallow spherical shells. *Journal of Applied Mechanics*, 28(4):557–562, 1961. doi: [10.1115/1.3641782](https://doi.org/10.1115/1.3641782).
- [16] N.C. Huang. Unsymmetrical buckling of thin shallow spherical shells. *Journal of Applied Mechanics* 31(3):447–457, 1964. doi: [10.1115/1.3629662](https://doi.org/10.1115/1.3629662).
- [17] H.J. Weinitschke. On asymmetric buckling of shallow spherical shells. *Journal of Mathematics and Physics*, 44(1–4):141–163, 1965. doi: [10.1002/sapm1965441141](https://doi.org/10.1002/sapm1965441141).

- [18] A. Holston. Approximate analytical solutions of the finite-deflection equations for a shallow spherical shell. *Journal of Applied Mechanics*, 34(1):65–72, 1964. doi: [10.1115/1.3607670](https://doi.org/10.1115/1.3607670).
- [19] F. Kikuchi, H. Ohya, and Y. Ando. Application of finite element method to axisymmetric buckling of shallow spherical shells under external pressure. *Journal of Nuclear Science and Technology*, 10(6):339–347, 1973. doi: [10.1080/18811248.1973.9735431](https://doi.org/10.1080/18811248.1973.9735431).
- [20] F. Zhou, Z. Chen, C. Zheng, F. Xu, Y. Hu, S. Hou, and Z. Qin. Experimental and numerical buckling failure analysis of acrylic hemispheres for application in neutrino detector. *Engineering Failure Analysis*, 78:147–160, 2017. doi: [10.1016/j.engfailanal.2017.03.017](https://doi.org/10.1016/j.engfailanal.2017.03.017).
- [21] H.N.R. Wagner, C. Hühne, J. Zhang, W. Tang, and R. Khakimova. Geometric imperfection and lower-bound analysis of spherical shells under external pressure. *Thin-Walled Structures*, 143:106195, 2019. doi: [10.1016/j.tws.2019.106195](https://doi.org/10.1016/j.tws.2019.106195).
- [22] Y. Wang, W. Tang, J. Zhang, S. Zhang, and Y. Chen. Buckling of imperfect spherical caps with fixed boundary under uniform external pressure. *Marine Structures*, 65:1–11, 2019. doi: [10.1016/j.marstruc.2019.01.004](https://doi.org/10.1016/j.marstruc.2019.01.004).
- [23] Y. Wang, J. Zhang, and W. Tang. Buckling Performances of Spherical Caps Under Uniform External Pressure. *Journal of Marine Science and Application*, 19(1):96–100, 2020. doi: [10.1007/s11804-020-00125-7](https://doi.org/10.1007/s11804-020-00125-7).
- [24] K.-Y. Yeh, W.-P. Song, and W.L. Cleghorn. Axisymmetric buckling of thin shallow circular spherical shells under uniform pressure for large values of geometric parameter λ . *International Journal of Non-Linear Mechanics*, 29(4):603–611, 1994. doi: [10.1016/0020-7462\(94\)90026-4](https://doi.org/10.1016/0020-7462(94)90026-4).
- [25] I.K. Silverman and J.R. Mays. A collocation solution of the nonlinear equations for axisymmetric bending of shallow spherical shells. *Journal of the Franklin Institute*, 294(3):181–192, 1972. doi: [10.1016/0016-0032\(72\)90013-0](https://doi.org/10.1016/0016-0032(72)90013-0).
- [26] H.J. Weinitschke. On the calculation of limit and bifurcation points in stability problems of elastic shells. *International Journal of Solids and Structures*, 21(1):79–95, 1985. doi: [10.1016/0020-7683\(85\)90106-4](https://doi.org/10.1016/0020-7683(85)90106-4).
- [27] W.T. Koiter. *A Translation of the Stability of Elastic Equilibrium*. Technical Report AFFDL-TR-70-25, pages 1-325, Ohio, 1970.
- [28] A. Lee, F.L. Jiménez, J. Marthelot, J. W. Hutchinson, and P.M. Reis. The Geometric Role of Precisely Engineered Imperfections on the Critical Buckling Load of Spherical Elastic Shells. *Journal of Applied Mechanics*, 83(11):11005, 2016. doi: [10.1115/1.4034431](https://doi.org/10.1115/1.4034431).
- [29] J. Zhang, Y. Wang, F. Wang, and W. Tang. Buckling of stainless steel spherical caps subjected to uniform external pressure. *Ships and Offshore Structures*, 13(7):779–785, 2018. doi: [10.1080/17445302.2018.1459358](https://doi.org/10.1080/17445302.2018.1459358).
- [30] N.K. Gupta, N.M. Sheriff, and R. Velmurugan. Experimental and theoretical studies on buckling of thin spherical shells under axial loads. *International Journal of Mechanical Sciences*, 50(3):422–432, 2008. doi: [10.1016/j.ijmecsci.2007.10.002](https://doi.org/10.1016/j.ijmecsci.2007.10.002).
- [31] M. Shariati and H.R. Allahbakhsh. Numerical and experimental investigations on the buckling of steel semi-spherical shells under various loadings. *Thin-Walled Structures*, 48(8):620–628, 2010. doi: [10.1016/j.tws.2010.03.002](https://doi.org/10.1016/j.tws.2010.03.002).
- [32] Y.-C. Tseng, P. Amon, L.M. Dolbachiian, and J.-Y. Juang. Guided buckling of elastoplastic spherical shells induced by indenters of various shapes. *Extreme Mechanics Letters*, 44:101247, 2021. doi: [10.1016/j.eml.2021.101247](https://doi.org/10.1016/j.eml.2021.101247).
- [33] D.P. Updike and A. Kalnins. Axisymmetric behavior of an elastic spherical shell compressed between rigid plates. *Journal of Applied Mechanics*, 37(3):635–640, 1970. doi: [10.1115/1.3408592](https://doi.org/10.1115/1.3408592).
- [34] D.P. Updike and A. Kalnins. Axisymmetric postbuckling and nonsymmetric buckling of a spherical shell compressed between rigid plates. *Journal of Applied Mechanics*, 39(1):172–177, 1972. doi: [10.1115/1.3422607](https://doi.org/10.1115/1.3422607).

- [35] R. Kitching, R. Houlston, and W. Johnson. A theoretical and experimental study of hemispherical shells subjected to axial loads between flat plates. *International Journal of Mechanical Sciences*, 17(11-12):693–703, 1975. doi: [10.1016/0020-7403\(75\)90072-7](https://doi.org/10.1016/0020-7403(75)90072-7).
- [36] V. Brizmer, Y. Zait, Y. Kligerman, and I. Etsion. The effect of contact conditions and material properties on elastic-plastic spherical contact. *Journal of Mechanics of Materials and Structures*, 1(5):865–879, 2006. doi: [10.2140/jomms.2006.1.865](https://doi.org/10.2140/jomms.2006.1.865).
- [37] V. Brizmer, Y. Kligerman, and I. Etsion. The effect of contact conditions and material properties on the elasticity terminus of a spherical contact. *International Journal of Non-Linear Mechanics*, 43(18-19):5736–5749, 2006. doi: [10.1016/j.ijsolstr.2005.07.034](https://doi.org/10.1016/j.ijsolstr.2005.07.034).
- [38] A. Ovcharenko, G. Halperin, G. Verberne, and I. Etsion. In situ investigation of the contact area in elastic-plastic spherical contact during loading-unloading. *Tribology Letters*, 25(2):153–160, 2007. doi: [10.1007/s11249-006-9164-y](https://doi.org/10.1007/s11249-006-9164-y).
- [39] L. Li, L. Wang, I. Etsion, and F. Talke. The effect of contact conditions and material properties on plastic yield inception in a spherical shell compressed by a rigid flat. *International Journal of Solids and Structures*, 48(3-4):463–471, 2011. doi: [10.1016/j.ijsolstr.2010.10.015](https://doi.org/10.1016/j.ijsolstr.2010.10.015).
- [40] L. Li, I. Etsion, A. Ovcharenko, and F.E. Talke. The onset of plastic yielding in a spherical shell compressed by a rigid flat. *Journal of Applied Mechanics*, 78(1):011016, 2011. doi: [10.1115/1.4001994](https://doi.org/10.1115/1.4001994).
- [41] S. Ronen, R. Goltsberg, and I. Etsion. A comparison of stick and slip contact conditions for a coated sphere compressed by a rigid flat. *Friction*, 5(3):326–338, 2017. doi: [10.1007/s40544-017-0178-2](https://doi.org/10.1007/s40544-017-0178-2).
- [42] P.K. Gupta and N.K Gupta. A study of axial compression of metallic hemispherical domes. *Journal of Materials Processing Technology*, 209(4):2175–2179, 2009. doi: [10.1016/j.jmatprotec.2008.05.004](https://doi.org/10.1016/j.jmatprotec.2008.05.004).
- [43] A. Nasto, A. Ajdari, A. Lazarus, A. Vaziri, and P.M. Reis. Localization of deformation in thin shells under indentation. *Soft Matter*, 9(29):6796–6803, 2013. doi: [10.1039/c3sm50279a](https://doi.org/10.1039/c3sm50279a).
- [44] A. Nasto and P.M. Reis. Localized structures in indented shells: A numerical investigation. *Journal of Applied Mechanics*, 81(12):21008, 2014. doi: [10.1115/1.4028804](https://doi.org/10.1115/1.4028804).
- [45] M. Shariati and M.M. Rokhi. Numerical and experimental investigations on buckling of steel cylindrical shells with elliptical cutout subject to axial compression. *Thin-Walled Structures*, 46(11):1251–1261, 2008. doi: [10.1016/j.tws.2008.02.005](https://doi.org/10.1016/j.tws.2008.02.005).
- [46] R. Degenhardt, K. Rohwer, W. Wagner, and J.-P. Delsenne. Postbuckling and collapse analysis of CFRP stringer stiffened panels – A GARTEUR activity. In *Proceeding of the 4th International Conference of Thin-Walled Structures ICTWS*, pages 121–128, Loughborough, England, 2004. doi: [10.1201/9781351077309-10](https://doi.org/10.1201/9781351077309-10).
- [47] R. Degenhardt and J.P. Delsenne. Buckling and postbuckling analysis of a CFRP stiffened panel for a better material exploitation. In *Proceeding of SAMTECH Users Conference*, pages 1–7, Paris, Frankreich, 2005.
- [48] J. Btachat. Buckling of shallow spherical caps subjected to external pressure. *Journal of Applied Mechanics*, 72(5):803–806, 2005. doi: [10.1115/1.1993667](https://doi.org/10.1115/1.1993667).
- [49] E. Reissner. Stresses and small displacements of shallow spherical shells. I. *Studies in Applied Mathematics*, 25(1–4):80–85, 1946. doi: [10.1002/sapm194625180](https://doi.org/10.1002/sapm194625180).
- [50] R.H. Homewood, A.C. Brine, and A.E. Johnson. Experimental investigation of the buckling instability of monocoque shells. *Experimental Mechanics*, 1(3):88–96, 1961. doi: [10.1007/BF02324071](https://doi.org/10.1007/BF02324071).
- [51] G.A. Thurston and F.A. Penning. Effect of axisymmetric imperfections on the buckling of spherical caps under uniform pressure. *AIAA Journal*, 4(2):319–327, 1966. doi: [10.2514/3.3435](https://doi.org/10.2514/3.3435).
- [52] M. Sunakawa and K. Ichida. A high precision experiment on the buckling of spherical caps subjected to external pressure. *ISAS report/Institute of Space and Aeronautical Science, University of Tokyo*, pages 87–121, Tokyo, 1974.

-
- [53] T. Kobayashi, Y. Mihara, and F. Fujii. Path-tracing analysis for post-buckling process of elastic cylindrical shells under axial compression. *Thin-Walled Structures*, 61:180–187, 2012. doi: [10.1016/j.tws.2012.05.018](https://doi.org/10.1016/j.tws.2012.05.018).
- [54] T. Kobayashi and Y. Mihara. Postbuckling analyses of elastic cylindrical shells under axial compression. In *Transactions of the Japan Society of Mechanical Engineers, Part A*, 77:582–589, 2011. doi: [10.1299/kikaia.77.582](https://doi.org/10.1299/kikaia.77.582). (in Japanese).
- [55] E. Riks. The application of Newton’s method to the problem of elastic stability. *Journal of Applied Mechanics*, 39(4):1060–1065, 1972. doi: [10.1115/1.3422829](https://doi.org/10.1115/1.3422829).
- [56] E. Riks. An incremental approach to the solution of snapping and buckling problems. *International Journal of Solids and Structures*, 15(7):529–551, 1979. doi: [10.1016/0020-7683\(79\)90081-7](https://doi.org/10.1016/0020-7683(79)90081-7).
- [57] E. Riks. Some computational aspects of the stability analysis of nonlinear structures. *Computer Methods in Applied Mechanics and Engineering*, 47:219–259, 1984. doi: [10.1016/0045-7825\(84\)90078-1](https://doi.org/10.1016/0045-7825(84)90078-1).
- [58] P. Jasion and K. Magnucki. Elastic buckling of barrelled shell under external pressure. *Thin-Walled Structures*, 45(4):393–399, 2007. doi: [10.1016/j.tws.2007.04.001](https://doi.org/10.1016/j.tws.2007.04.001).
- [59] M.A. Krenzke and T.J. Kiernan. Elastic stability of near-perfect shallow spherical shells. *AIAA Journal*, 1(12):2855–2857, 1963. doi: [10.2514/3.2187](https://doi.org/10.2514/3.2187).